1996

Control Systems Architecture, Navigation, and Communication Research Using the NPS Phoenix Underwater Vehicle

Control Systems Architecture, Navigation, and Communication Research Using the NPS Phoenix Underwater Vehicle

D. B. Marco, A. J. Healey[1], R. B. McGhee, D. P. Brutzman, R. Cristi
Autonomous Underwater Vehicles Laboratory
Naval Postgraduate School
Monterey, CA. 93943

[1] Point of Contact
(408)-656-3462(Ph.)
(408)-656-2238 (Fax)
healey@me.nps.navy.mil

1. Introduction

While there has always been a need to determine the global position of an underwater vehicle, in some missions involving search, mapping, and intervention with objects, navigation to local area landmarks is more appropriate and precise. All aspects of autonomous search have been of interest to us for some time now, and we have recently developed and extended our robot control system architecture using Prolog as a rule based mission specification language to drive vehicle missions involving motion around targets of interest. In particular, we have studied the use of onboard scanning sonar to perform local area navigation. Additionally, we have installed a new low cost short / long baseline acoustic communications / navigation system called DiveTracker, and are developing filtering software that would combine inputs from several sources having different update rates and levels of precision to produce high update rate navigational information with the precision afforded by the low update rate reference. Also, the DiveTracker system affords a low cost acoustic communications system that can be used

for low rate message sending and retrieval from autonomous vehicles. In this paper, we attempt to give an elaborate analysis of local area maneuvering using sonar based feature detection from the local scene. A mathematical model of the vehicle response is used to provide control inputs during periods when sonar updates are not available and the experimental results indicate that this method will supplement other techniques where positioning precision to centimeters is necessary. In the second and third parts of the paper, we outline some recent results of our experiments in Monterey Bay using the Systron Donner Motion Pak inertial system corrected by differential GPS when surfaced. The navigation system is smoothed and coordinated through a complementary filter that bounds the normal drift in free inertial systems. Lastly, some recent work on an examination of message passing using IP protocol through seawater with the 'DiveTracker' system will be discussed.

2. Background

Recent developments in underwater robotics are aimed at providing solutions to the problems of commercial, scientific, and military missions in the coastal ocean environment. Small autonomous vehicles will be able to monitor, search and survey areas of the ocean floor in shallow water. Providing results in near to real time, supervised autonomous activity including mission replanning and system reconfiguration can be used to inspect and monitor underwater structures, harbor environments, and obtain minefield reconnaissance data.

Two classes of mission arise. The survey mission requires an energy efficient vehicle to cruise and follow designated way points whilst taking relevant oceanographic data. The second (the intervention mission) requires a vehicle capable of slow speed and even

station keeping with thrusters and servo control to objects using vision, sonar, tactile sensors, or combinations thereof. Examples of survey vehicles include the Odyssey [1], and the Ocean Voyager [2], Remus [3] and the larger vehicles such as the Draper UUV [4] and the Navy's LDUUV [5], while examples of thruster controlled vehicles include the OTTER [6], the Phoenix [7], the Marius [8] and Vortex [9], and the entire class of Remotely Operated Vehicles called ROV's [10].

In the class of vehicles designed for the intervention mission, Marks, et. al. [6] have studied the problem of servo positioning the OTTER vehicle to visual cues from stereoscopic cameras although monocular video data was used to perform edge detection and servo control of the pan and tilt mounting coupled to the vehicle platform. Some of the co-authors of this paper have reported positioning control of the Phoenix vehicle to acoustic returns from high frequency (1.2Mhz.) sonar where the sonar was integrated into the execution level control software [11] as necessary to the stabilization of the vehicle motion. Part of the problem lies in the need for improved modeling of thruster behavior as described in Yoerger [12], and Healey et. al. [13]. Once maneuvering control around objects in the local area scene is understood to a satisfactory degree, intervention using manipulators and other tactile devices will be enabled. Such activities as changing out a battery pack for a bottom mounted sensor or finding and entering an underwater garage for repowering will then become commonplace.

We focus first on the problem of local area navigation and maneuvering using model based control and acoustic feature extraction techniques for precise positioning.

3. Model Based Control Formulation

Absent of an inertial position reference, where sonar position updates are asynchronous, and occur at times much longer than the control frequency of 10 Hz, a dynamic model of the vehicle is used for state information between updates. A three degree-of-freedom model (longitudinal, lateral, and heading) is used since the motion is restricted to the horizontal plane with the depth maintained by a separate controller. The model is given by including drag, added mass, and steady state thrust and for surge is

$$M_x \dot{u}(t) + b_x u(t)|u(t)| = 2\mathsf{a}_x \mathrm{v}_x(t)|\mathrm{v}_x(t)| \tag{1}$$

The sway directional equation of motion is

$$M_y \dot{v}(t) + b_y v(t)|v(t)| = \mathsf{a}_y \mathrm{v}_{blt}(t)|\mathrm{v}_{blt}(t)| + \mathsf{a}_y \mathrm{v}_{slt}(t)|\mathrm{v}_{slt}(t)| \tag{2}$$

and finally the yaw equation of motion becomes

$$I_z \dot{r}(t)(\mathrm{t}) + b_{\mathsf{y}} r(t)|r(t)| = \mathsf{a}_{\mathsf{y}} \mathrm{v}_{blt}(t)|\mathrm{v}_{blt}(t)| - \mathsf{a}_{\mathsf{y}} \mathrm{v}_{slt}(t)|\mathrm{v}_{slt}(t)| \tag{3}$$

where

$$M_x = m + m_{ax}, \quad M_y = m + m_{ay}, \quad I_z = I_{zz} + I_{azz}$$

and

$$\mathrm{v}_x(t)|\mathrm{v}_x(t)| = (\mathrm{v}_{ls}(t)|\mathrm{v}_{ls}(t)| + \mathrm{v}_{rs}(t)|\mathrm{v}_{rs}(t)|)/2$$

m is the vehicle mass, I_{zz} the mass moment of inertia about the body-fixed z-axis, and the subscript "*a*" refers to the added mass or inertia of the body. $u(t)$, $v(t)$, and $r(t)$ are the body-fixed rates for longitudinal (x-axis), lateral (y-axis), and heading (y)

directions. b_x, b_y, b_y are the square-law damping coefficients, $v_{ls}(t)$, $v_{rs}(t)$, and $v_{blt}(t)$, $v_{slt}(t)$ are the thruster motor input voltages for the left/right rear screws, and the bow/stern lateral thrusters respectively. The voltage to force/moment coefficients are given by a_x, a_y, and a_y.

The above dynamics equations can be formulated using matrix notation as

$$\boldsymbol{M}\dot{\boldsymbol{x}}(t) = \boldsymbol{f}(\boldsymbol{x}(t), \boldsymbol{b}) + \boldsymbol{g}(a)\boldsymbol{u}(t) \tag{4}$$

and vehicle kinematics are defined by

$$\dot{\boldsymbol{z}}(t) = \boldsymbol{h}(y)\boldsymbol{x}(t) + \boldsymbol{u}_c(t). \tag{5}$$

The body-fixed rates are

$$\boldsymbol{x}(t) = \{u(t)\ v(t)\ r(t)\}^T,$$

and the global position and orientation is given by

$$\boldsymbol{z}(t) = \{X(t)\ Y(t)\ y(t)\}^T.$$

The vector describing the hydrodynamic drag that is a function of the body-fixed rates and square-law damping coefficients, $\boldsymbol{b} = \{b_x\ b_y\ b_y\}$ is

$$\boldsymbol{f}(\boldsymbol{x}(t), \boldsymbol{b}) = \{-b_x u(t)|u(t)| - b_y v(t)|v(t)| - b_y r(t)|r(t)|\}^T,$$

the mass matrix is

$$\boldsymbol{M} = \begin{bmatrix} M_x & 0 & 0 \\ 0 & M_y & 0 \\ 0 & 0 & I_z \end{bmatrix},$$

and input gain matrix which is solely a function of the thruster coefficients, $\mathbf{a} = \{ a_x \; a_y \; a_y \; \}$ is

$$\boldsymbol{g}(\mathbf{a}) = \begin{bmatrix} 2a_x & 0 & 0 \\ 0 & a_y & a_y \\ 0 & a_y & -a_y \end{bmatrix}.$$

Finally, the control input vector is defined as

$$\boldsymbol{u}(t) = \{ v_x(t) | v_x(t) | \; v_{blt}(t) | v_{blt}(t) | \; v_{slt}(t) | v_{slt}(t) | \}^T . \tag{6}$$

For the case of translation in X, Y and rotation ψ, the transformation matrix from the body-fixed axes to the global reference is given by

$$\boldsymbol{h}(\psi(t)) = \begin{bmatrix} cos(\psi(t)) & -sin(\psi(t)) & 0 \\ sin(\psi(t)) & cos(\psi(t)) & 0 \\ 0 & 0 & 1 \end{bmatrix}, \tag{7}$$

and it's time derivative is

$$\dot{\boldsymbol{h}}(\psi(t), \dot{\psi}(t)) = \begin{bmatrix} -\dot{\psi}(t) sin(\psi(t)) & -\dot{\psi}(t) cos(\psi(t)) & 0 \\ \dot{\psi}(t) cos(\psi(t)) & -\dot{\psi}(t) sin(\psi(t)) & 0 \\ 0 & 0 & 0 \end{bmatrix}.$$

Any current disturbances are represented by

$$\boldsymbol{u}_c(t) = \{ u_c(t) \; v_c(t) \; r_c(t) \}^T$$

where the elements $\boldsymbol{u}_c(t)$ are the body-fixed current rates.

The sliding mode control law can now be formulated defining the tracking error vector in terms of global coordinates as

$$\begin{bmatrix} \dot{\tilde{\boldsymbol{z}}}(t) \\ \tilde{\boldsymbol{z}}(t) \end{bmatrix} = \begin{bmatrix} \dot{\boldsymbol{z}}_{com}(t) \\ \boldsymbol{z}_{com}(t) \end{bmatrix} - \begin{bmatrix} \dot{\boldsymbol{z}}(t) \\ \boldsymbol{z}(t) \end{bmatrix}. \tag{8}$$

The subscript "*com*" refers to the commanded value of the position or rate in question, where commanded time variations of states must be consistent with vehicle physical capabilities and usually come from separate path planning algorithms.

Since the dynamics equation is in terms of body-fixed rates and accelerations, Equation (8) can be expressed in terms of body-fixed rates using Equation (5). If $\boldsymbol{u}_c(t)$ is assumed zero:

$$\begin{bmatrix} \boldsymbol{h}(\mathsf{y}(t))\tilde{\boldsymbol{x}}(t) \\ \tilde{\boldsymbol{z}}(t) \end{bmatrix} = \begin{bmatrix} \boldsymbol{h}(\mathsf{y}(t))\boldsymbol{x}_{com}(t) \\ \boldsymbol{z}_{com}(t) \end{bmatrix} - \begin{bmatrix} \boldsymbol{h}(\mathsf{y}(t))\boldsymbol{x}(t) \\ \boldsymbol{z}(t) \end{bmatrix}. \tag{9}$$

Now that the tracking error has been formulated, an equation defining the sliding surface in terms of this error can be written as

$$\mathsf{s}(\tilde{\boldsymbol{x}}(t), \tilde{\boldsymbol{z}}(t)) = \begin{bmatrix} \boldsymbol{S}_1 & \boldsymbol{S}_2 \end{bmatrix} \begin{bmatrix} \boldsymbol{h}(\mathsf{y}(t))\tilde{\boldsymbol{x}}(t) \\ \tilde{\boldsymbol{z}}(t) \end{bmatrix} \tag{10}$$

where

$$\mathbf{s}(\tilde{\boldsymbol{x}}(t),\tilde{\boldsymbol{z}}(t)) \in \Re^{3\times 1}; \quad \boldsymbol{S}_1, \boldsymbol{S}_2 \in \Re^{3\times 3}$$

The elements of $\boldsymbol{S}_1$ and $\boldsymbol{S}_2$ can be selected to provide the desired performance of the closed loop system. For the case of planar control, these become

$$\boldsymbol{S}_1 = \begin{bmatrix} 1 & 0 & 0 \\ 0 & 1 & 0 \\ 0 & 0 & 1 \end{bmatrix} \qquad \boldsymbol{S}_2 = \begin{bmatrix} \mathrm{I}_x & 0 & 0 \\ 0 & \mathrm{I}_y & 0 \\ 0 & 0 & \mathrm{I}_y \end{bmatrix}$$

To ensure that stable tracking behavior is achieved, the condition:

$$\frac{lim}{t\to\infty} \dot{\mathbf{s}}(\tilde{\boldsymbol{x}}(t),\tilde{\boldsymbol{z}}(t)) \to 0$$

with

$$\frac{lim}{t\to\infty} \mathbf{s}(\tilde{\boldsymbol{x}}(t),\tilde{\boldsymbol{z}}(t)) \to 0$$

will also imply

$$\tilde{\boldsymbol{x}}(t),\tilde{\boldsymbol{z}}(t) \to 0 \quad \text{as} \quad t\to\infty .$$

The condition that $\mathbf{s}(\tilde{\boldsymbol{x}}(t),\tilde{\boldsymbol{z}}(t))$ is always decreasing can be established if a Lyapunov function of the sliding surface is formed as

$$V(t) = \frac{1}{2}\mathbf{s}^T(\tilde{\boldsymbol{x}}(t),\tilde{\boldsymbol{z}}(t)) * \mathbf{s}(\tilde{\boldsymbol{x}}(t),\tilde{\boldsymbol{z}}(t)), \tag{11}$$

and

$$\dot{V} = \dot{\mathbf{s}}'(\tilde{\boldsymbol{x}}(t),\tilde{\boldsymbol{z}}(y)) * \mathbf{s}(\tilde{\boldsymbol{x}}(t),\tilde{\boldsymbol{z}}(y)) \tag{12}$$

Global asymptotic stability is guaranteed if $V(t)$ is positive definite and $\dot{V}(t)$ is negative definite. The quadratic nature of (11) assures the positive definiteness of $V(t)$, while negative definiteness of $\dot{V}(t)$ may be met by,

$$\dot{\sigma}_i(\tilde{x}(t),\tilde{z}(t)) = -\eta_i \, sgn(\sigma_i(\tilde{x}(t),\tilde{z}(t))) \quad i = x, y, \psi \tag{13}$$

where each η_i is a positive scalar matched with each control direction, x, y, and ψ. The positive definiteness of $V(t)$ and the negative definiteness of $\dot{V}(t)$, implies that given any initial condition, $\sigma(\tilde{x}(0),\tilde{z}(0))$, $\sigma(\tilde{x}(t),\tilde{z}(t))$ will remain bounded such that

$$V(\sigma(\tilde{x}(t),\tilde{z}(t)) \le V(\sigma(\tilde{x}(0),\tilde{z}(0)).$$

Since $sgn(\sigma_i(\tilde{x}(t),\tilde{z}(t)))$ is discontinuous across $\sigma(\tilde{x}(t),\tilde{z}(t)) = 0$, undesirable switch chattering can occur. This is alleviated by the use of a "boundary layer" around zero. Therefore, instead of using a sgn function, a continuous form is preferred such that

$$sat(\sigma_i(\tilde{x}(t),\tilde{z}(t))./\phi_i) = \begin{cases} sgn(\sigma_i(\tilde{x}(t),\tilde{z}(t))) & if \left|\sigma_i(\tilde{x}(t),\tilde{z}(t))\right| > \phi_i \\ \sigma_i(\tilde{x}(t),\tilde{z}(t))/\phi_i & otherwise \end{cases}$$

where "./" denotes element by element division. Another approach is to simply use the continuous function $tanh(\sigma(\tilde{x}(t),\tilde{z}(t)))$. Substituting the definition of sat into Equation (13) and noting Equation (10), it can be written in a more compact form as

$$\dot{\sigma}(\tilde{x}(t),\tilde{z}(t)) = S_1 \dot{h}(\psi(t))\tilde{x}(t) + S_1 h(\psi(t))\dot{\tilde{x}}(t) + S_2 \dot{\tilde{z}}(t) = -F(\sigma(\tilde{x}(t),\tilde{z}(t)),\phi) \tag{14}$$

Substituting the dynamics equation (1) into (14) yields the control solution $u(t)$ and since the matrices $f(\bullet)$, $g(\bullet)$, and $h(\bullet)$ are uncertain in general, they must be formulated

using estimates, denoted as $\hat{\boldsymbol{f}}(\bullet)$, $\hat{\boldsymbol{g}}(\bullet)$, and $\hat{\boldsymbol{h}}(\bullet)$, where the $(\bullet)$ is used for notational compactness. The control vector can be split into three parts

$$\boldsymbol{u}(t)=\boldsymbol{u}_1(t)+\boldsymbol{u}_2(t)+\boldsymbol{u}_3(t)$$

where

$$\boldsymbol{u}_1(t)=\hat{\boldsymbol{g}}(\bullet)^{-1}(\hat{\boldsymbol{M}}\dot{\boldsymbol{x}}_{com}(t)-\hat{\boldsymbol{f}}(\bullet)) \tag{15}$$

contains the acceleration terms,

$$\boldsymbol{u}_2(t)=\hat{\boldsymbol{g}}(\bullet)^{-1}\hat{\boldsymbol{M}}\hat{\boldsymbol{h}}^{-1}(\bullet)(\dot{\hat{\boldsymbol{h}}}(\bullet)\hat{\boldsymbol{h}}(\bullet)^{-1}+\boldsymbol{S}_1^{-1}\boldsymbol{S}_2)\dot{\tilde{\boldsymbol{z}}}(t) \tag{16}$$

contains the velocity terms, and finally

$$\boldsymbol{u}_3(t)=\hat{\boldsymbol{g}}(\bullet)^{-1}\hat{\boldsymbol{M}}\hat{\boldsymbol{h}}^{-1}(\bullet)\boldsymbol{S}_1^{-1}\boldsymbol{F}(\mathsf{s}(\bullet),\mathsf{f}) \tag{17}$$

is the switching term, where

$$\dot{\boldsymbol{x}}_{com}(t)=\hat{\boldsymbol{h}}^{-1}(\bullet)(-\dot{\hat{\boldsymbol{h}}}(\bullet)\hat{\boldsymbol{h}}(\bullet)^{-1}\dot{\boldsymbol{z}}_{com}(t)+\ddot{\boldsymbol{z}}_{com}(t))$$

$\boldsymbol{S}_1$ is identity, and if all commanded velocities and accelerations are zero the control reduces to

$$\begin{aligned}\boldsymbol{u}_1(t)&=\hat{\boldsymbol{g}}(\bullet)^{-1}\hat{\boldsymbol{f}}(\bullet)\\ \boldsymbol{u}_2(t)&=-\hat{\boldsymbol{g}}(\bullet)^{-1}\hat{\boldsymbol{M}}\hat{\boldsymbol{h}}^{T}(\bullet)[\dot{\hat{\boldsymbol{h}}}(\bullet)\hat{\boldsymbol{h}}^{T}(\bullet)+\boldsymbol{S}_2)\hat{\dot{\boldsymbol{z}}}(t)\\ \boldsymbol{u}_3(t)&=\hat{\boldsymbol{g}}(\bullet)^{-1}\hat{\boldsymbol{M}}\hat{\boldsymbol{h}}^{T}(\bullet)\boldsymbol{F}(\mathsf{s}(\bullet),\mathsf{f})\end{aligned} \tag{18}$$

where $\boldsymbol{u}_1(t)$, $\boldsymbol{u}_2(t)$, and $\boldsymbol{u}_3(t)$ contain the acceleration, velocity and switching terms respectively.

4. Target Detection with Sonar

To perform local area navigation using sonar, it is necessary to select an easily discernible feature in the vehicle operating area and use it as a fixed reference. The target feature should be stationary and reasonably unique with respect to other structures in the sonar field of view. This will be necessary to enable repeatable and unambiguous detection of the reference feature. In order to classify these features, each must be segmented into a separate object and analyzed to see if it posses the structural properties of the desired target for reference.

For the results presented in this paper, the target used for the local navigation reference was a 0.5 meter diameter, 0.75 meter long cylinder placed vertically in the water column of the NPS AUV test tank which measures 6.0 by 6.0 meters square and 1.8 meters deep. A Tritech ST1000 profiling sonar head was used which is mounted vertically in the nose of the NPS Phoenix vehicle. The head uses a stepper motor, which can mechanically rotate the transducer through 360^{o} with respect to it's mounting at a minimum angular resolution of 0.9^{o}. For each step, the sonar is pinged and a single range value is returned which enables a complete profile of the area surrounding the vehicle to be constructed.

An actual scan of the cylindrical target and square tank walls is shown in Figure 2. A sweep width of $\pm 35^{o}$ and angular resolution of 1.8^{o} was used. Each dot or "pixel" corresponds to a discrete range value returned by the sonar for a given angular position of

the transducer head. Several disjoint groups or segments of pixels are visible in the field of view: the two sections of the tank wall, and the cylinder which casts an acoustic shadow against the wall. Since sonar range drop outs and noise are common with sonars, the tank wall to the upper right of the cylinder is broken up into several segments, although in reality, it is a continuous feature. It is this nature of acoustic sensors that lead to the development of the following algorithms for cylinder detection in the NPS test tank.

Since the cylinder is the desired target for the local area reference, returns from the tank walls need to be filtered out and ignored. This can be accomplished by segmenting each contiguous, disjoint group of range pixels and analyzing them for the desired characteristics of a cylinder. The method to isolate these segments is outlined in the flow diagram in Figure 3. The filter is initialized by pinging at a fixed bearing to obtain an average range value, $\bar{r}$. Once this is done, the head is commanded to scan in a clockwise direction and each range return is first tested for feasibility. If the range is zero or if it exceeds the maximum operating range, r_{max}, it is ignored and that range, r_i, is set to the current average range, $\bar{r}$, and the scan proceeds. If the range is feasible, a test is performed to see if it lies within an error band of $\pm \Delta r$ of the average and if so, the value of $\bar{r}$ is recalculated using the new range. The range and the associated bearing angle is then stored in a vector of size n, (the number of pixels defining the segment). If the range falls outside of the error band, a flag is set to examine how closely subsequent returns compare to the new range. A secondary average, $\bar{r}_{new}$, is initialized to this value and a new segment is declared if the next n_{min} adjacent ranges are consistent with this average at which time the current average is set to $\bar{r}_{new}$. The old segment is now terminated at $i - n_{min}$ and the range, bearing and pixel count values are processed to extract any shape information they may provide. If the subsequent ranges, less than n_{min} pixels are inconsistent with $\bar{r}_{new}$, and fall near the previous average, a new segment is not assumed

and the scan continues using $\bar{r}$. These "false alarms" occur quite frequently due to the nature of the sonar returns which contain drop outs and false ranges. The value of n_{min} can be varied depending on the environment of operation. For the test tank which provides relatively clean signals, the value of n_{min} is typically 3, but in more noisy conditions, a larger value should be used to provide higher filtering.

Once a separate segment has been identified, the vector containing it's ranges and bearing angles is analyzed. The flow diagram for this algorithm is shown in Figure 4. To determine if the object defined by the segment is a cylinder, it must posses the following characteristics:

1. Consist of a sufficient number of pixels, n, that does not exceed a maximum, n_{max}. If the number of pixels is large, in this case greater than 10 it can be safely assumed the segment is a wall due the relative size of the cylinder.

2. Be in front of the tank walls. This is an obvious observation since the cylinder is assumed to be in the tank but must be included in the algorithm to avoid confusion by perceived cylindrical shaped areas on the wall due to noise.

3. Have a central range closer than it's edges. Since a cylinder appears the same from any direction in a horizontal plane, the center of the segment will always be closer the sonar than the beginning and ending edges.

The preceding algorithms have been used with much success in the NPS test tank and should operate well in an open water environment especially since the tank walls will be

absent and the reference target the most visible object in the area. This procedure can be modified to search for other geometric shapes since the idea of segmentation of each feature is retained but does not attempt to supplant more sophisticated and robust pattern recognition algorithms available. This method was adopted since it can be executed in real time and is simply used as a means to perform the tasks described in the following sections.

5. Relative Position Estimation

Once the reference target has been identified, it becomes the origin of the navigation coordinate frame where the X-axis is aligned with heading 0 degrees and the Y-axis along a heading of 90^{o} as shown in Figure 5. The two dimensional position vector to the origin of the vehicle body-fixed reference with respect to the navigation frame at detection time T is

$$\boldsymbol{R}_v(T) = \begin{Bmatrix} X_v(T) \\ Y_v(T) \end{Bmatrix} = -\left(\boldsymbol{r}_s(T) + \boldsymbol{R}_{cyl}(T) \right) \tag{19}$$

where

$$\boldsymbol{r}_s(T) = \boldsymbol{h}(\boldsymbol{\psi}(T)) \begin{Bmatrix} x_s \\ y_s \end{Bmatrix},$$

and x_s, y_s is the position of the sonar head in vehicle coordinates.

$$\boldsymbol{R}_{cyl}(T) = \begin{Bmatrix} (R_{cyl}(T) + r_{cyl}) cos(\boldsymbol{\psi}(T) + \boldsymbol{\psi}_s(T)) \\ (R_{cyl}(T) + r_{cyl}) sin(\boldsymbol{\psi}(T) + \boldsymbol{\psi}_s(T)) \end{Bmatrix} \tag{20}$$

where $R_{cyl}(T)$ is the sonar range to the target, $\psi_s(T)$ is the heading angle of the sonar beam, and for the case of a cylindrical target, r_{cyl} is it's radius. After the target has been found, and the location of the vehicle is determined, the sonar is commanded to sweep across it at a prescribed angular sweep width denoted ψ_{sw} about a heading which is the center of the target. This reduces the amount of delay time between re-acquiring the target.

6. Position Update

Since there is a delay time of up to 10 seconds between successive target detection, the vehicle control must use a dynamic model between position updates. Equation 4 is integrated to obtain estimates of the vehicle position denoted $\hat{X}(t)$, and $\hat{Y}(t)$ during this time. The scan direction command angle $\psi_{sd}(t)$ between position updates is computed using

$$\psi_{sd}(t) = atan2\left(\frac{-(\hat{Y}(t) + x_s sin(\psi(t)) + y_s cos(\psi(t)))}{-(\hat{X}(t) + x_s cos(\psi(t)) + y_s sin(\psi(t)))}\right) - \psi(t) \qquad (21)$$

and a maneuver using this approach is shown in Figure 6. If the target has not been reaquired within a specified time, the head is commanded to return to continuous sweep mode. This is needed if the scan width is too narrow and there exists a large discrepancy between the model and the actual vehicle, the scan direction calculated from the estimates of position can be in error. One approach to reduce this possibility is to increase the scan width, ψ_{sw} to say 120^o degrees but doing this will increase the time between updates and has not been done for this series of experiments.

For vehicle control in a plane, the complete state is defined by

$$\boldsymbol{X}(t)=\{u(t)\,v(t)\,r(t)\,X(t)\,Y(t)\,\psi(t)\}^{T}$$

and the block diagram representation of the control scheme is shown in Figure 7. When the cylinder has been identified, the model is asynchronously updated at time of target detection using a Kalman filter of the form

$$\hat{X}(T)=(1-K)\hat{X}^{-}(t)+KX_{v}(T)$$

$$\hat{Y}(T)=(1-K)\hat{Y}^{-}(t)+KY_{v}(T) \tag{22}$$

where

$$K=\frac{\sigma_{m}^{2}}{\sigma_{m}^{2}+\sigma_{s}^{2}} \tag{23}$$

and σ_{m}^{2} is the variance of the system model estimate of position and σ_{s}^{2} is the variance of vehicle position using the sonar. $\hat{X}^{-}(t)$, and $\hat{Y}^{-}(t)$ is the current estimate of position from the model just before the correction from the sonar is obtained. This analysis assumes the position estimate from the sonar is extremely accurate and the model very inaccurate. Therefore, the variance for position from sonar is set to 0 and infinity for the model. This causes the current estimate from the model to be disregard at the time of sonar update and

reduces Equation (22) to be simply

$$\hat{X}(t)=KX_{v}(t)$$

$$\hat{Y}(t)=KY_{v}(t) \tag{24}$$

which states complete confidence in the sonar. At this time the dynamic model of the system is reset to the values obtained from Equation (24) and the model updates from there during the next interval between updates.

The onboard gyroscopes provide the heading angle and yaw rate values at 10 Hz, which are synchronous and highly accurate and no estimation of these is required. The observation vector is defined by

$$\boldsymbol{y}(t) = \boldsymbol{C}\boldsymbol{X}(t) \tag{25}$$

where the observation matrix is

$$\boldsymbol{C} = \begin{bmatrix} 0 & 0 & 0 & 0 & 0 & 0 \\ 0 & 0 & 0 & 0 & 0 & 0 \\ 0 & 0 & 1 & 0 & 0 & 0 \\ 0 & 0 & 0 & 0 & 0 & 0 \\ 0 & 0 & 0 & 0 & 0 & 0 \\ 0 & 0 & 0 & 0 & 0 & 1 \end{bmatrix}.$$

With only these two measurements made, Equation (25) reduces to

$$\boldsymbol{y}(t) = \begin{Bmatrix} r(t) \\ \mathbf{y}(t) \end{Bmatrix} \tag{26}$$

which is used each time step in the vehicle controller and dynamic model.

7. Experimental Results

A five pose experiment was performed in the NPS hover tank. During execution, all pertinent data was collected, including depth and heading information, all sonar data, and the estimates of position, position rate, and the updates from the sonar. Table 1 shows the commanded position and heading comprising the five poses and are shown in Figure 8.

Table 1. Commanded Mission Poses

Pose	X_{com} (m)	Y_{com} (m)	ψ_{com} (rad)
1	2.13	-2.13	0.0
2	2.13	0.0	0.0
3	2.13	2.13	0.0
4	2.13	0.0	0.5236
5	-2.74	-2.13	0.0

The following tables give the parameter values used in the vehicle model and the sliding mode controller gains.

Table 2. Parameters for Vehicle Model

Parameter	Value	Unit
m	194.88	Kg
m_{ax}	19.49	Kg
m_{ay}	155.90	Kg
I_{zz}	53.60	Kg-m^2
I_{zza}	53.60	Kg-m^2
b_x	63.80	Kg/m
b_y	815.46	Kg/m
b_ψ	74.86	Kg-m^2
a_x	0.056	N/V^2
a_y	0.018	N/V^2
a_ψ	0.008	N-m/V^2

Table 3. Sliding Mode Controller Gains

Parameter	Value	Unit
λ_x	0.20	rad/sec
λ_y	0.20	rad/sec
λ_ψ	0.20	rad/sec
η_x	0.15	m/sec^2
η_y	0.09	m/sec^2
η_ψ	0.20	rad/sec^2
ϕ_x	0.06	m/sec
ϕ_y	0.09	m/sec
ϕ_ψ	0.20	rad/sec

Note: $\alpha_{slt} = \alpha_{blt} = \alpha_y l_{lt}$, where l_{lt} is the distance from the mass center of the vehicle to the center of the lateral thruster axes which is the same for both thrusters.

The experiment specified the vehicle to submerge to a depth of 0.4 meters using vertical thrusters as detailed in [14]. Once this depth was reached, the ST1000 sonar was activated and scanned clockwise until the target (cylinder) was identified. At this time, the first pose (1) was issued and the vehicle started the controlled maneuver.

Most control phase transitions of the Phoenix are event based, meaning that a certain set of criteria must be met in order for a transition to occur. A common example of this is when a position set point is sent to the vehicle controllers and reached. A method of determining whether the vehicle has indeed reached this point must be programmed into the control logic. Measuring the position error alone and declaring the maneuver complete when this error is small is not sufficient. This is because the vehicle could be overshooting the commanded position and simply passing through the set point. Therefore, not only must the position error be small but the rate error must also be small. This dual criteria can be expressed mathematically as a positive definite, linear combination of the position error $\boldsymbol{e}$ and the position rate error $\dot{\boldsymbol{e}}$, such that

$$= \begin{Bmatrix} \sigma_X \\ \sigma_Y \\ \sigma_y \end{Bmatrix} = w_e |\boldsymbol{e}| + w_{\dot{e}} |\dot{\boldsymbol{e}}| \tag{27}$$

where w_e and $w_{\dot{e}}$ are weights for the position and rate errors respectively and for planar motion the errors are

$$\boldsymbol{e} = \begin{Bmatrix} X_{com} - X_v \\ Y_{com} - Y_v \\ \psi_{com} - \psi \end{Bmatrix} \quad \text{and} \quad \dot{\boldsymbol{e}} = \begin{Bmatrix} \dot{X}_{com} - \dot{X} \\ \dot{Y}_{com} - \dot{Y} \\ r_{com} - r \end{Bmatrix}$$

This equation allows a minimum value of σ for each control direction X, Y, and ψ denoted, σ_{0X}, σ_{0Y}, and $\sigma_{0\psi}$ to be specified defining a threshold for the combination of errors which can be set relatively large when precision control is not required or low for extremely precise positioning. Once each σ drops below it's respective σ_0, the maneuver is declared complete and a transition to the next control phase may occur.

For these experiments, the transition was based on position errors from the sonar ranges, not from the model estimates since the model will always predict a very smooth trajectory to the set point. The parameters for the error equation used were $\sigma_{0X} = \sigma_{0Y} =$ 0.08 meters, $\sigma_{0\psi} = 0.1$ radians, and $w_e = w_{\dot{e}} = 1.0$.

Figure 9 shows the position response results where the upper trace is $\hat{Y}(t)$ and the lower $\hat{X}(t)$. The position, calculated from sonar at update, $X_v(T)$ and $Y_v(T)$ are shown with circles and asterisks respectively. Examining the response for $\hat{X}(t)$ it is evident that the model for the longitudinal direction is in error since the predicted position at the time of correction is about double that calculated with the sonar. This mismatch has been attributed to the absence of shrouds around the rear screws. Without them, an unmodeled transient force lag is present that is common with open propellers. Since this lag was uncompensated, and the control was dictated by the model predictions between position updates, large voltage commands to the screws were of too short a duration to build up sufficient force on the vehicle as shown in Figure 10. The performance was further degraded by the estimated position and rate feedback from the model. As these values were assumed to be nearing the set point pose, the controller actually reversed the

propellers (negative voltage command) in an attempt to slow the vehicle. This effect can also be clearly seen in Figure 10 between the time 46.1 seconds and 53.1 seconds, the time of the position update from the sonar. The prediction of the lateral movement, $\hat{Y}(t)$, is much better since the cross-body thrusters are shrouded due to their tunnel design and the model parameters are well established. Model / sonar update differences were attributed to an unknown current that was identified between successive updates This allows compensation for model errors and external disturbances. In all, local dynamic positioning to centimeters is possible in the tank environment.

8. GPS / INS Navigation

Another aspect of our work relates to precise underwater and near surface navigation of AUVs using a combination of inertial, acoustic, and GPS navigation. In order to carry out such research in a realistic context, we have constructed an instrumented tow-fish containing a small, low cost inertial measurement unit (IMU) and a GPS antenna [15]. To date, data collected in Monterey Bay suggests that submerged navigation for periods of several minutes is possible with less than 10 meters rms. error using only water speed sensing and a magnetic compass to aid pure inertial navigation. We have also shown that when on-line error estimates indicate the need for inertial reset, this can be accomplished to a precision of about 1 meter rms. This precision is obtained using locally derived differential GPS even in moderate sea states with an antenna extending only a few inches above the ocean surface [16]. Further at sea testing of this system will be reported in [17]. This work will investigate further accuracy improvements attainable by a low cost small size acoustic Doppler measurement of velocity over ground or with respect to the water column. By further developments in Kalman filtering for these small units that is based on complementary high and low frequency filters we would expect that both high frequency updates with low frequency

corrections will allow compensation of disturbances induced by wave motion for precision positioning and global precision to DGPS accuracy.

9. Acoustic Communications and Navigation

Recently, the Phoenix AUV has undergone a hardware upgrade to enable open water testing in the Moss Landing harbor facilities of MBARI. This upgrade involved adding differential GPS, an acoustic short / long baseline navigation, communications and tracking system (Dive-Tracker), and a Sun Voyager notebook workstation as a second internal vehicle computer. The Sun Voyager processes the Strategic and Tactical level software while linkage to the Execution level software employs internal ethernet socket communications. These changes have allowed us to move from our fresh water test pool to a more useful and realistic *salt-water* environment. Results obtained from experiments in salt water to date have shown that it is indeed possible to send IP protocol communications through seawater using the Dive-Tracker system [18], even though the data rate and distance are not large. Also, for local area positioning, the Phoenix has used a short baseline technique in the Moss Landing harbor area, giving precision to tens of centimeters with range to over 100 m. These results will be reported in six M.S. theses to be completed by NPS students in March 1996, and summarized in [19].

10. Discussion and Conclusion

The results of these experiments have shown that it is possible to navigate an underwater vehicle in a local area using an acoustic sensor for position information. The accuracy of the model used between updates is moderately satisfactory and can allow for time varying currents. However, some additional model adjustments could be made to

compensate for the force lag in the longitudinal direction during transient thrust conditions. This undesirable effect could also be alleviated by the addition of shrouds around the rear screws which should bring the performance up to that of the lateral thrusters. While these results were taken in a tank environment, another improvement would be to fuse the model with an INS system in between updates from the sonar and then fuse that estimate with the sonar data to obtain a smoother averaging at update time. This would allow for compensation of wave induced disturbances, while retaining the positioning precision found. Since the sonars are mechanically scanned, and a delay of up to 10 seconds between position update is common, use of an electronically scanned or multi-beam sonars may be preferable although our experience to date has been that cross-talk between beams can be a serious problem.

11. References

[1] Bellingham, J. G., Goudey, C. A., et. al. "A Second Generation Survey AUV", Proc. *IEEE Symp. on Autonomous Underwater Vehicle Technology*, July 1994, pp. 148-156.

[2] Smith, S. M., Dunn, S., "The Ocean Voyager II: An AUV Designed for Coastal Oceanography", Procs. *IEEE Symp. on Autonomous Underwater Vehicle Technology*, July 1994, pp. 139-148

[3] Von Alt, C., Allen, B., Austin, T., Stokey, R., "Remote Environmental Measuring Units" *Proceedings of the IEEE Symposium on Autonomous Underwater Vehicle Technology*, AUV '94, July 1994, pp. 13-20.

[4] Brancart, C., "The Evolution of the DARPA / ARPA UUV Program", *Proceedings of the 1994 NSF IARP Workshop on Mobile Robots for Subsea Environments*, MBARI, Pacific Grove, CA. May 1994.

[5] Agoras, C., Lee, C. O., Hills, S., Carlino, D., "U. S. Navy UUV Navigation", *Sea Technology*, January, 1996, pp. 56-60.

[6] Marks, R. L., Rock, S. M., Lee, M. J., "Real Time Video Mosaicking of the Ocean Floor",.*Procs. IEEE Symp. on Auton. Underwater Vehicle Tech.*, July 1994, pp. 21-28.

[7] Healey, A.J., Marco, D. B., "Slow Speed Flight Control of Autonomous Underwater Vehicles: Experimental Results with NPS AUV II" *Proceedings of the 2nd International Offshore and Polar Engineering Conference*, San Francisco, July 14-19 1992.

[8] Pascoal, A., "The AUV MARIUS: Mission Scenarios, Vehicle Design, Construction and Testing", *Proceedings of the 2nd Workshop on Mobile Robotics for Subsea Environments*, Monterey bay Aquarium, Monterey, California, May 1994.

[9] Perrier, M., Rigaud, V., Peuch, A., Coste-Maniere, E., Simon, B., " Vortex: A versatile Testbed Vehicle for Control Algorithms Evaluation", *Proceedings of the 8th. UUST*, Durham New Hampshire, September 27-29, 1993, pp. 29-36.

[10] Newman, J. B., Stakes, D.1994, "Tiburon: Development of an ROV for Ocean Science Research ", *Proc. OCEANS'94*, Brest, France Sept. 1994, Vol. II pp. 483-488.

[11] Healey, A. J., et al., "Coordination of the Hovering Behaviors of the NPS AUV II using Onboard Sonar Servoing", *Proceedings of the 1994 NSF IARP Workshop on Mobile Robots for Subsea Environments*, MBARI, Pacific Grove, CA. May 1994 .

[12] Yoerger, D.R., Cooke, J.G., Slotine, J.J.E., "The Influence of Thruster Dynamics on Underwater Vehicle Behavior and Their Incorporation into Control System Design" *IEEE Journal of Oceanic Engineering*, Vol. 15, No. 3, 1991, pp. 167-178

[13] Healey, A. J., Rock, S. M., Cody, S., Miles, D., Brown, J. P., " Towards an Improved Understanding of Thruster Dynamics for Underwater Vehicles", *IEEE Journal of Oceanic Engineering* Oct. 1995, Vol. 20, No. 4, pp. 354-361.

[14] Healey, A. J., Marco, D. B., McGhee, R.B., "Autonomous Underwater Vehicle Control Coordination Using A Tri-Level Hybrid Software Architecture", *Proceedings of the IEEE Robotics and Automation Conference*, Minneapolis, MI, April 1996.

[16] McGhee, R.B., et al., "An Experimental Study of an Integrated GPS/INS System for Shallow-Water AUV Navigation (SANS)", *Proc. of 9th International Symposium on Unmanned Untethered Submersible Technology*, Univ. of New Hampshire, Durham, NH, Sept. 25-27, 1995, pp. 153-167.

[17] Bachmann, E. R., and Gay, D. L., *Design and Evaluation of an Integrated GPS/INS System for Shallow-Water AUV Navigation*, MS. Thesis, Naval Postgraduate School, Monterey, CA, September, 1995.

[17] Bachmann, E. R., et al., "Evaluation of an Integrated GPS/INS System for Shallow-Water AUV Navigation (SANS)", *Proceedings of the IEEE Symposium on Autonomous Underwater Vehicle Technology*, Monterey, CA, June, 1996.

[18] Reimers, S. *"Towards Internet Protocol Over Seawater: Forward Error Correction Using Hamming Codes for Reliable Acoustic Telemetry"*, MS Thesis, Naval Postgraduate School, Monterey, CA. September 1995.

[19] Brutzman, D. P., et. al. "NPS Phoenix Software Integration and Open Water Testing ", *Proceedings of the IEEE Symposium on Autonomous Underwater Vehicle Technology*, AUV96 Monterey, CA. June 3-6, 1996.

List of Figures

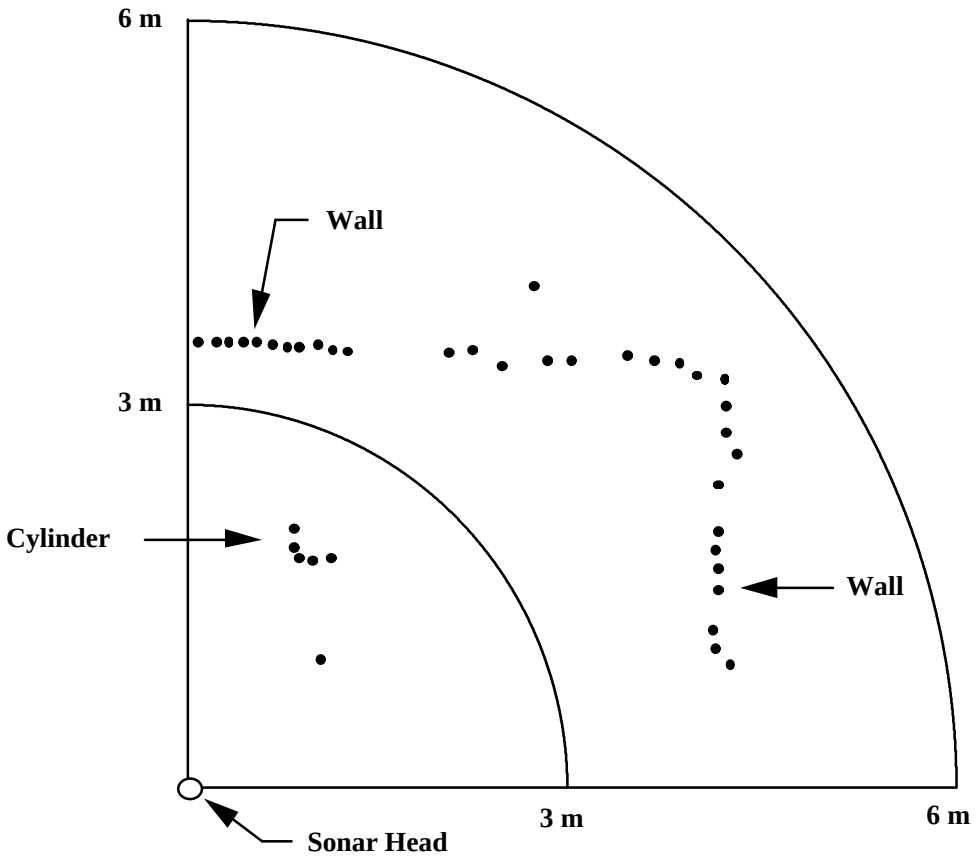
6 m
Wall
3 m
Cylinder
Wall
3 m
6 m
Sonar Head

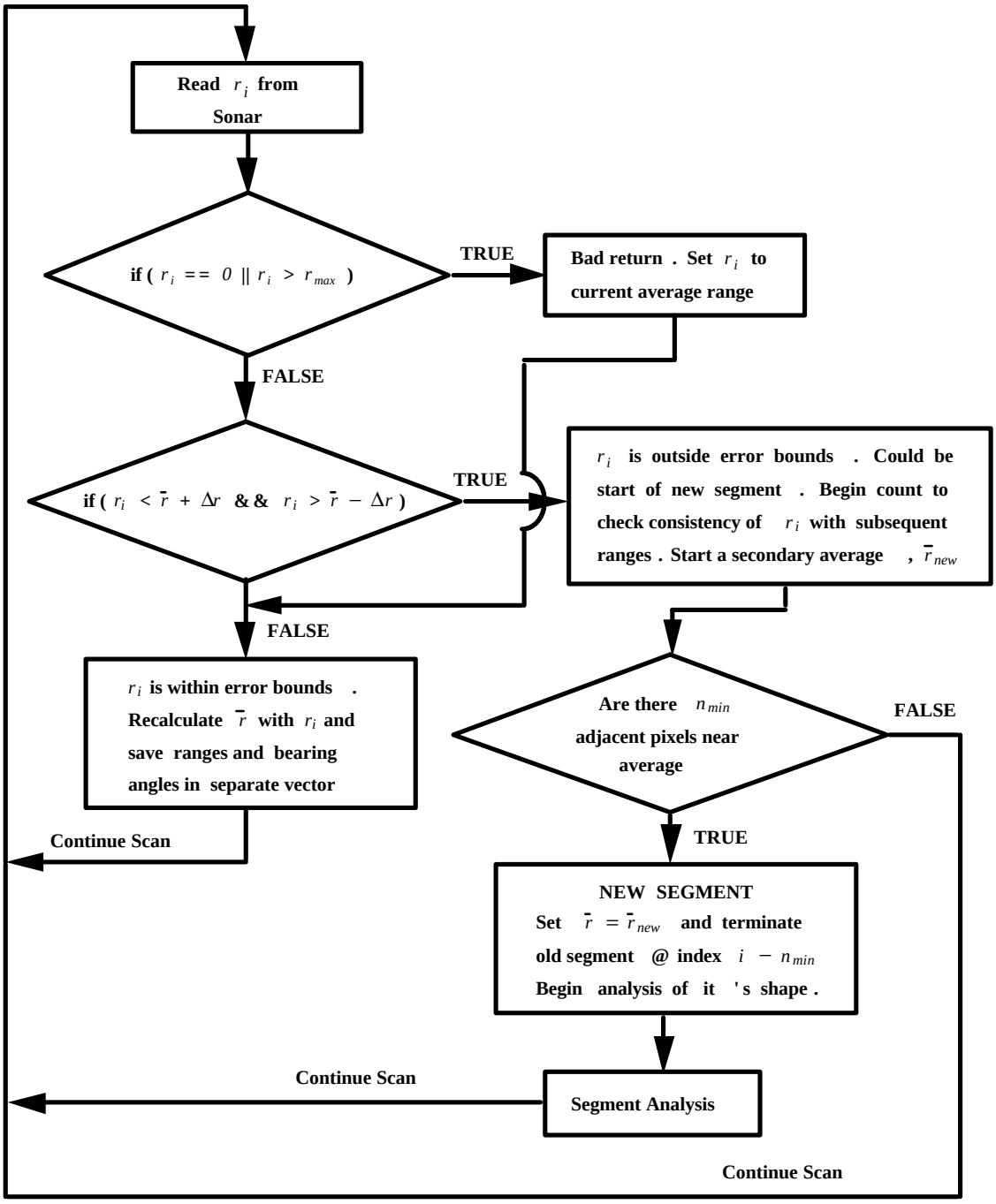
Read r_i from Sonar
if ($r_i == 0 \,||\, r_i > r_{max}$)
TRUE
Bad return . Set r_i to current average range
FALSE
if ($r_i < \bar{r} + \Delta r$ && $r_i > \bar{r} - \Delta r$)
TRUE
r_i is outside error bounds . Could be start of new segment . Begin count to check consistency of r_i with subsequent ranges . Start a secondary average , $\bar{r}_{new}$
FALSE
r_i is within error bounds . Recalculate $\bar{r}$ with r_i and save ranges and bearing angles in separate vector
Continue Scan
Are there n_{min} adjacent pixels near average
FALSE
TRUE
NEW SEGMENT
Set $\bar{r} = \bar{r}_{new}$ and terminate old segment @ index $i - n_{min}$
Begin analysis of it 's shape .
Continue Scan
Segment Analysis
Continue Scan

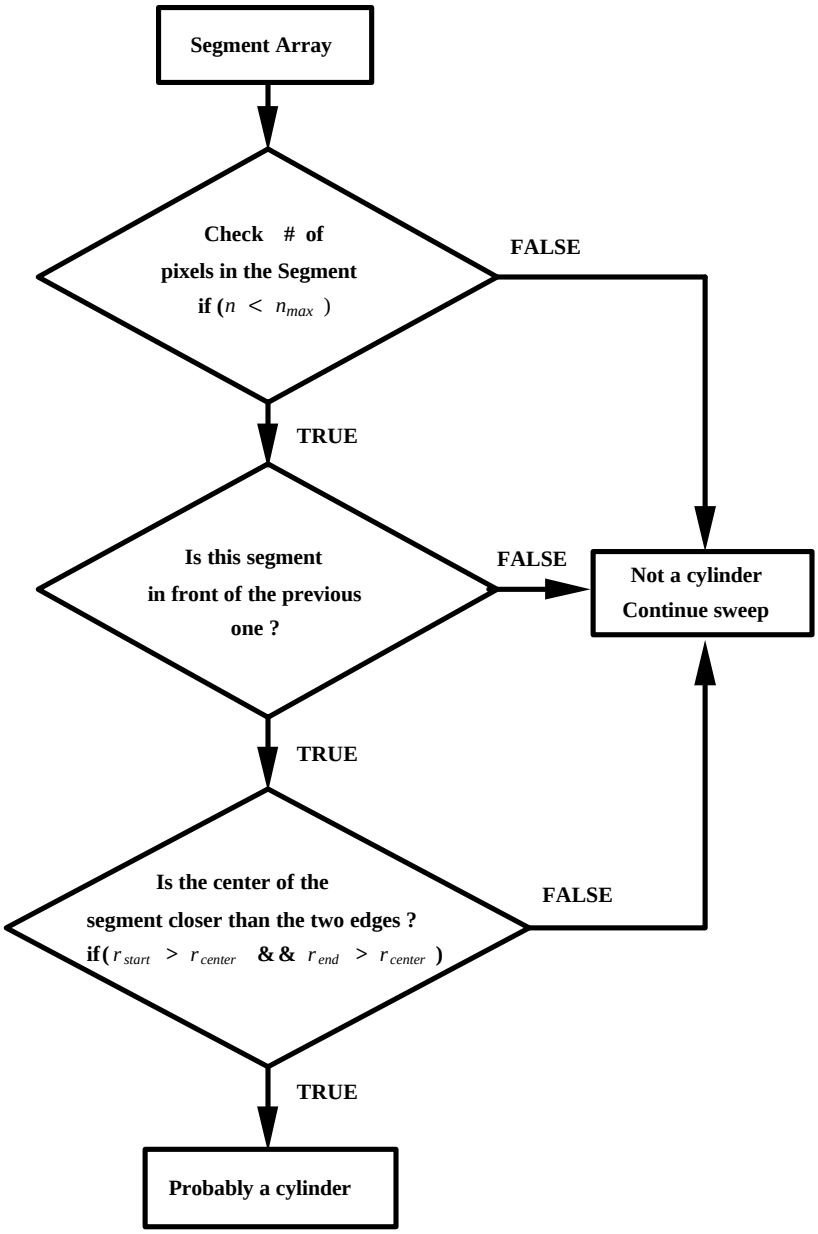
Segment Array
Check # of
pixels in the Segment
if ($n < n_{max}$)
FALSE
TRUE
Is this segment
in front of the previous
one ?
FALSE
Not a cylinder
Continue sweep
TRUE
Is the center of the
segment closer than the two edges ?
if ($r_{start} > r_{center}$ && $r_{end} > r_{center}$)
FALSE
TRUE
Probably a cylinder

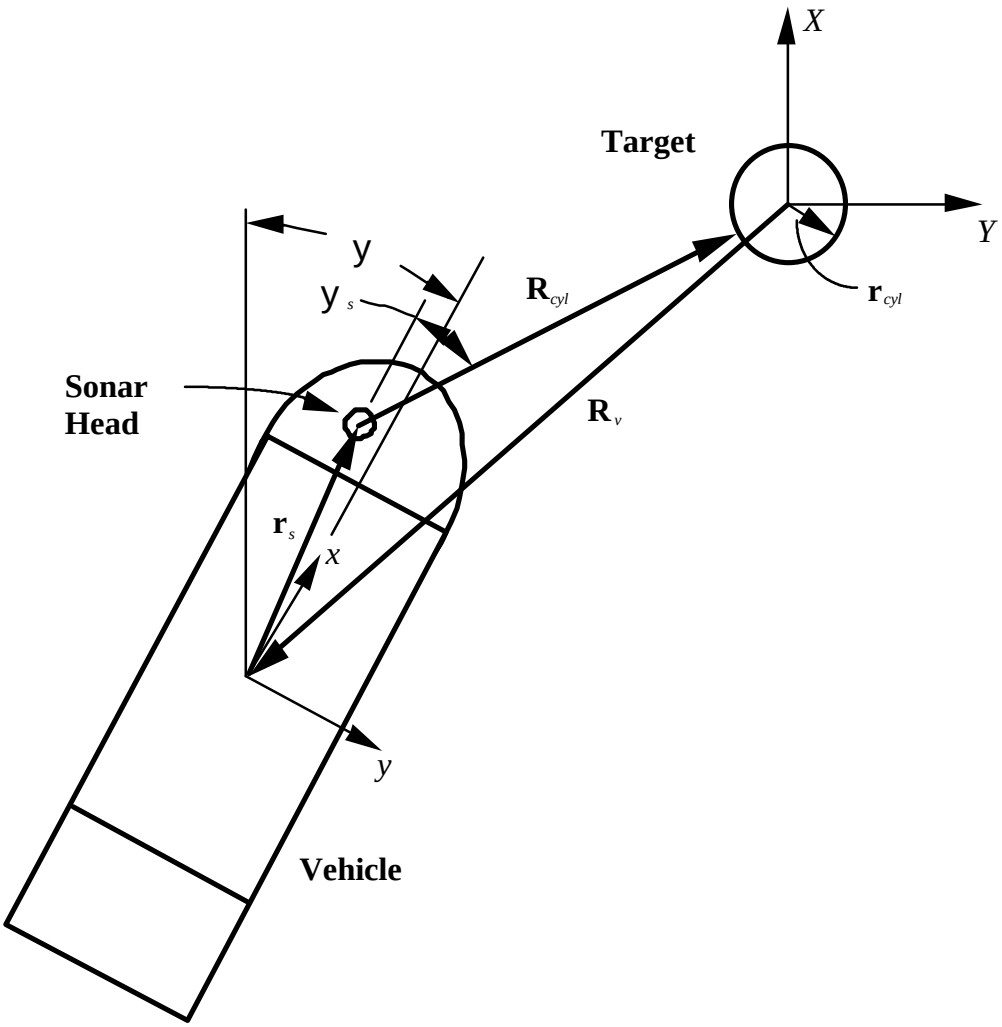
X
Target
Y
y
y_s
$\mathbf{R}_{cyl}$
$\mathbf{r}_{cyl}$
Sonar
Head
$\mathbf{R}_v$
$\mathbf{r}_s$
x
y
Vehicle

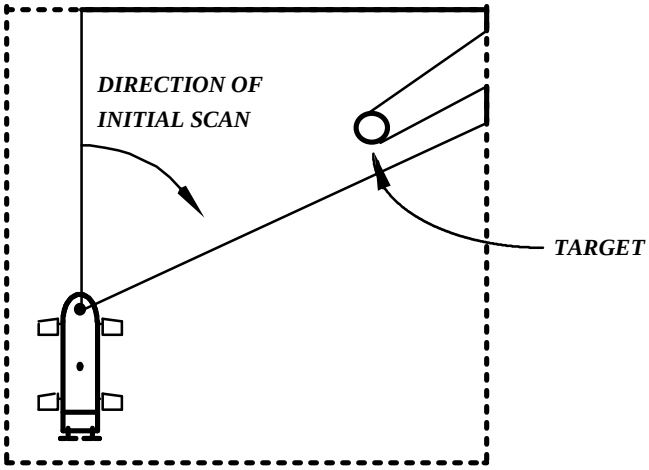

1

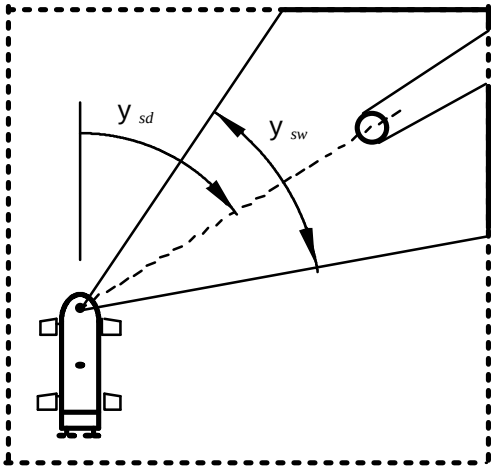

2

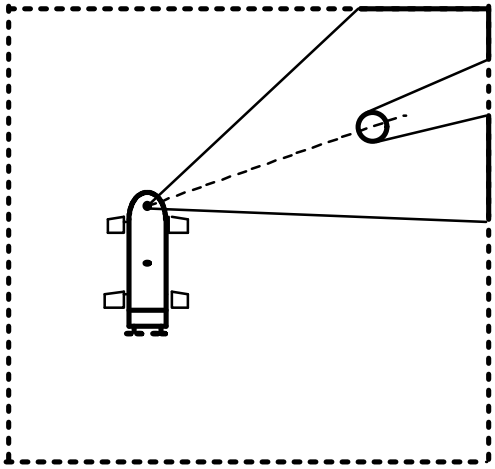

3

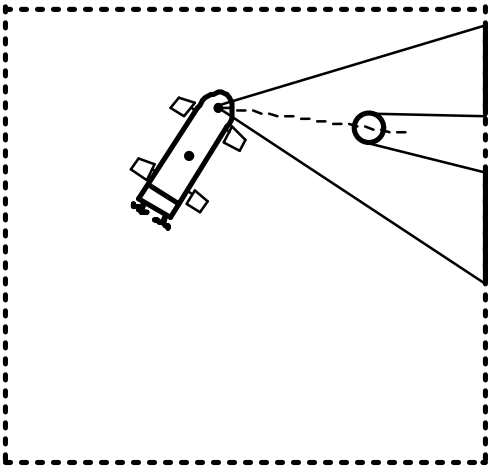

4

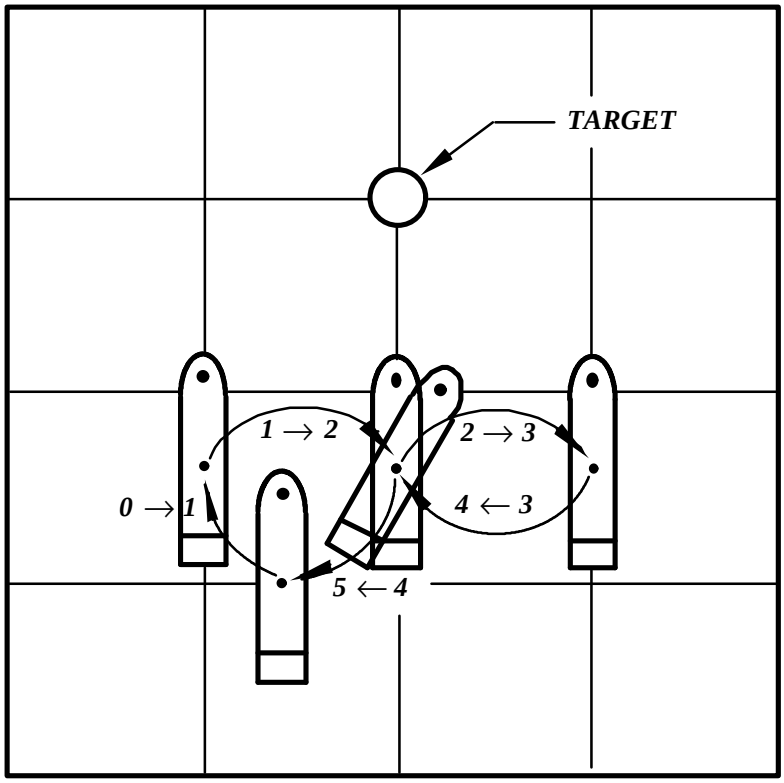
TARGET
1 → 2
2 → 3
0 → 1
4 ← 3
5 ← 4

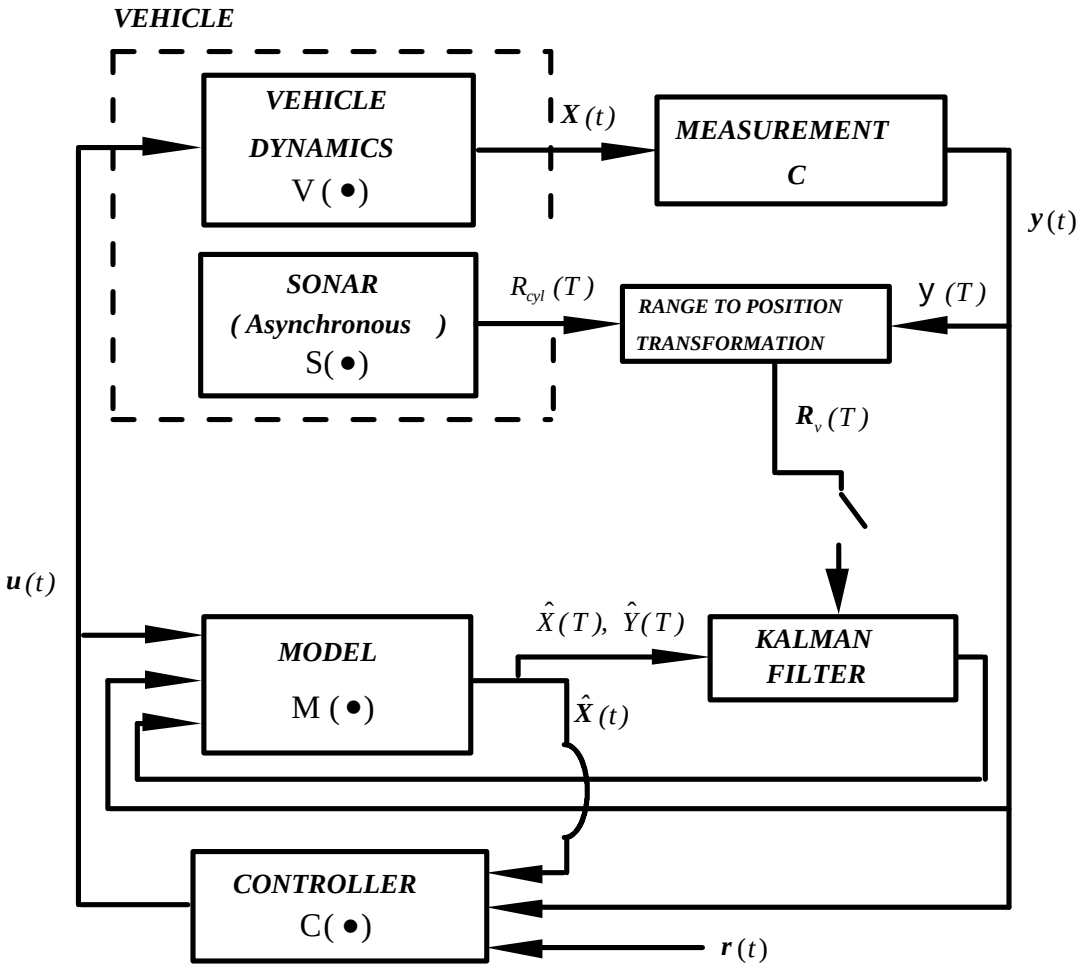
VEHICLE
VEHICLE DYNAMICS
V (•)
X (t)
MEASUREMENT
C
y (t)
SONAR
(Asynchronous)
S(•)
R_cyl (T)
RANGE TO POSITION TRANSFORMATION
y (T)
R_v (T)
u (t)
MODEL
M (•)
X̂ (T), Ŷ (T)
KALMAN FILTER
X̂ (t)
CONTROLLER
C(•)
r (t)